An Investigation Into the Use of Geiger-Mode Solid-State Photomultipliers for Simultaneous PET and MRI Acquisition

Seong Jong Hong, In Chan Song, Mikiko Ito, Sun Il Kwon, Geon Song Lee, Kwang-Souk Sim, Kwang Suk Park, June Tak Rhee, and Jae Sung Lee

***Abstract*—Photon detecting Geiger-mode solid-state devices are being actively researched and developed because, unlike photomultiplier tubes (PMT), they can be used in high-magnetic-field and radio-frequency environments, such as in magnetic resonance imaging (MRI) scanners. In addition, some Geiger-mode solid-state devices have higher photon detection efficiencies than PMTs and higher gains than avalanche photo-diodes (APD). We tested Geiger-mode solid-state photomultipliers (SSPM) inside a 3 T MRI to study the possibility of using them in combined PET/MRI scanners. Approximately 16% energy resolutions and ~1.3 ns coincidence time resolutions with ^{22}Na and lutetium yttrium oxyorthosilicate (LYSO) were obtained for full-width at half maximum (FWHM) for T1, T2, and gradient echo T2* MRI pulse sequences with little MR image degradation. The study shows that SSPMs have excellent potential for use in combined PET/MRI scanners.**

***Index Terms*—MRI, multimodal imaging, PET, PET/MRI.**

I. Introduction

POSITRON emission tomography (PET) scanners, which enable quantitative measurements of physiological characteristics by the in-vivo imaging of biochemical substances, have been used to investigate biochemical and pathological phenomena, diagnose disease, and to determine prognosis after treatment. Magnetic resonance imaging (MRI) provides superb high soft-tissue contrast as compared with computer tomography (CT), and does not require the use of ionizing radiation, which is particularly beneficial for pediatric and pregnant patients [1]. Therefore, it is expected that combined PET/MRI scanners represent the future for biomedical imaging, and that these scanners will either supplement or compete with PET/CT for basic research and clinical applications [2], [3]. However, one major obstacle of the combined PET/MRI system with photomultiplier tubes (PMT) is that these tubes are extremely sensitive to even low magnetic fields, i.e., of only 20–30 gauss.

One of the proposed PET/MRI methods involves the transfer of light signals from scintillation crystals located inside an MRI, via long optical fibers, to PMTs located outside the magnetic field [4], [5]. The main limitation of this method is that energy resolution is degraded due to light loss during optical transfer. Simultaneous PET/MRI acquisition using PET detectors with the poor energy resolution caused by long optical fibers is not favorable in clinical environment because the large number of scattered photons that have not been removed sufficiently due to the poor energy resolution will degrade the quality and contrast of the PET image.

The use of semiconductor photo-detectors, such as avalanche photodiodes (APD), rather than PMTs offers an alternative development option which is currently being pursued by several research and commercial groups. APDs are compact and insensitive to magnetic fields as compared with PMTs, and these properties are desirable for PET/MRI [6]. Even though APDs have been successfully incorporated into small animal [7]–[9] and human brain PET/MRI units [10], [11], available APDs have low gains of an order of hundreds and thus require elaborate preamplifiers.

Geiger-mode solid-state devices are being developed for photon detection by several companies, and are referred to as Geiger-mode photo-detectors (GMPD), multi-pixel photon counters (MPPC), silicon photomultipliers (SiPM), and solid-state photomultipliers (SSPM). All of these devices consist of many mini-cells, each of which, when struck by a photon, generates an avalanche of electrons. Some of these devices have promising characteristics, e.g., relatively high gains ($\sim 10^6$) and high photon detection efficiencies (20~50%) at photon wavelengths of ~420 nm. Moreover, the high gains of these solid-state devices can be advantageous in harsh environments, such as in MRI scanners versus APDs. Other advantages of these solid-state devices include a fast pulse rise time of <1 ns, and significantly lower operating voltages of <100 V

Manuscript received January 22, 2008; revised March 6, 2008. This work was supported by grants from the Basic Research Program (R01-2006-000-10296-0) and the Atomic Energy R&D Program (Development of basic GMPD PET detector technology for PET/MRI) of the Korean Science and Engineering Foundation (KOSEF).

S. J. Hong is with the Institute of Radiation Medicine, Medical Research Center, Seoul National University, Seoul 110-744, Korea.

I. C. Song is with the Institute of Radiation Medicine, Medical Research Center, Seoul National University, Seoul 110-744, Korea. He is also with the Department of Diagnostic Radiology, Seoul National University College of Medicine, Seoul 110-744, Korea.

M. Ito and K.-S. Sim are with the Department of Physics, Korea University, Seoul 136-701, Korea.

S. I. Kwon is with the Department of Nuclear Medicine, Seoul National University College of Medicine, Seoul 110-744, Korea. He is also with the Interdisciplinary Programs in Radiation Applied Life Science Major, Seoul National University, Seoul 110-744, Korea.

G. S. Lee and K. S. Park are with the Department of Biomedical Engineering, Seoul National University College of Medicine, Seoul 110-744, Korea.

J. T. Ree is with the Department of Physics, Konkuk University, Seoul 143-701, Korea.

J. S. Lee is with the Institute of Radiation Medicine, Medical Research Center, Seoul National University, Seoul 110-744, Korea. He is also with the Departments of Nuclear Medicine and Biomedical Sciences, Seoul National University College of Medicine, Seoul 110-744, Korea (e-mail: jaes@snu.ac.kr).

Color versions of one or more of the figures in this paper are available at http://ieeexplore.ieee.org.

Digital Object Identifier 10.1109/TNS.2008.924082

TABLE I
SPECIFICATIONS OF THE SSPM (SSPM_0611B4MM_PCB)

Parameter	Unit	Typical Value
Peak sensitivity wavelength (λ_p)	nm	440
Single photon detection efficiency	%	25 at λ_p
Operating voltage	V	36
Efficient gain		$0.6{\times}10^5$
Signal rise time	ns	0.7
Number of micro-cells		1700
Fill or geometric factor	%	>70

compared to typical APDs and PMTs. The typical coincidence time resolution of APDs is on the order of a handful of ns [9]–[11], and the poor time resolution lead to higher numbers of random and multiple events in the data sample, causing the degradation of PET images and not be appropriate for PET scanners with a capability of time of flight (TOF).

The feasibility of the SiPM concept has been demonstrated in scintillation based PET scanner readout elements, where they achieved energy resolutions of about 22% and coincidence time resolutions of 2.1 ns [12]. In addition, we also found that SSPM (SSPM_0604BE_CER, Photonique SA, Switzerland) coupled with LYSO resulted in a 25% energy resolution and a 4.5 ns time resolution in combination with a ^{22}Na radiation source [13]. The SSPM used in our previous test has a single photon detection efficiency of 10% at 400 nm, a signal rise time of 5 ns and 556 micro-cells with a sensitive area of 1×1 mm^2. The previous test was measured with LYSO crystals of size of $1.5 \times 1.5 \times 7.0$ mm^3.

In this study, we tested a new SSPM (SSPM_0611B4MM_PCB) inside a 3 T MRI, 3.0T VH/i EXCITE E2M4 (GE, USA), to study its possible use in PET/MRI scanners. After describing the specifications of the SSPM, SSPM-LYSO couplings, and signal readout, we present the energy and coincidence time resolutions of SSPM-LYSO couplings exposed to a ^{22}Na positron source outside and inside the 3 T MRI. Then we present the energy and coincidence time resolutions of SSPM-LYSO couplings during the simultaneous acquisition of data with the 3 T MRI using various MRI sequences. Finally, MRI phantom images with and without the SSPM-LYSO couplings inside an 8-channel head coil were also compared.

II. MATERIALS AND METHODS

A. Geiger-Mode Solid-State Photomultipliers

The specifications of the SSPM_0611B4MM_PCB provided by the vendor are shown in Table I. Its sensitive area was 2×2 mm^2 and its packaging area 4.0×5.5 mm^2. Given the high single photon detection efficiency (25% at 440 nm) and the fast signal rise time of this device, it has the potential to deliver good energy and high temporal resolutions. Even though the gain of this unit was about a factor of 10 lower than that of the device (SSPM-0604BE-CER) we previously tested [13], its gain was much higher than those of typical APDs, and therefore, its output signals did not require elaborate preamplification.

B. SSPM-LYSO Couplings and Signal Readout

A Lucite structure was used to fix two SSPM-LYSO couplings. Each SSPM-LYSO coupling was constructed attaching a SSPM to a LYSO crystal of size of $2 \times 2 \times 10$ mm^2. We chose this crystal size to match the sensitive area of the SSPM. The LYSO crystal was wrapped with three layers of 3M enhanced spectral reflector (ESR) polymer except for the surface facing the SSPM. Optical grease (BC-630) of refractive index 1.463 was applied to the interface between the SSPM and the LYSO crystal. A 1.8×10^6 Bq ^{22}Na radiation source was positioned between two SSPM-LYSO couplings, at a distance of 3 mm from the face of each LYSO crystal. We did not bother precisely to align the SSPM-LYSO couplings and the radiation source since the precise measurement of event rates was not our purpose.

Since the amplifier obtained from Photonique SA produced positive signals, we added an extra capacitor and resistor to invert signals so that they were compatible with the VME/NIM system. We also added protective diodes, which limited voltages applied to the SSPMs to < 33 V, particularly during the simultaneous acquisition of SSPM-LYSO couplings with the 3 T MRI scanner. We applied 32.3 V to both SSPMs. The applied voltage was measured between the cathode and anode of the SSPM.

Only nonmagnetic electronic components were used, as were connectors to signal and power cables. PVC insulated cables were used for the power supply, and BNC cables for signal extraction. However, PVC insulated cables of length 30 cm were used from the electronics board to the BNC cables for easy shielding the circuit board with a copper sheet (thickness 0.15 mm) shielding box. Since the NIM/VME data acquisition system and power supplies to the SSPMs had to be located in the MRI controller room outside the MRI scanning room, signal cables of length 20.0 m were used to transfer signals to the NIM/VME system between the MRI room and the MRI controller room. Power supplies for the SSPMs and amplifier circuit boards were placed in the MRI controller room. 15 m long power cables were used to apply voltages to the SSPMs and amplifier circuit boards.

Fig. 1 shows the data flow diagram used for the test setup. Amplified signals were used to generate coincidence signals to measure charges and coincidence timings using NIM and VME modules. Appropriate lengths of cables were added to ensure that signals arrived within the ADC GATE of 300 ns and that TDC START pulses arrived before TDC STOP pulses. To discriminate signals and noise, we used a CAEN N485 NIM constant fraction discrimination module. In addition, we also used a CAEN V965 VME ADC module, which measures integrated charges of up to 800 pC with 200 fC/bit resolution. To measure arrival time differences between START and STOP pulses, we used a CAEN V775N VME TDC module, which measures time differences of up to 140 ns with 35 ps/bit resolution. The amplifier circuits were placed inside the copper sheet shielding box shown in Fig. 2.

C. Test of SSPM-LYSO Couplings Outside and Inside 3 T MRI

The Lucite structure for the SSPM-LYSO couplings and the radiation source were attached to the outside of the head coil, shown in Fig. 2, which also shows the copper-shield box alongside the head coil. This arrangement of the SSPM-LYSO couplings and the copper-shield box around the head coil was selected after considering likely crystal positioning and the positions of readout elements around the head coil. This

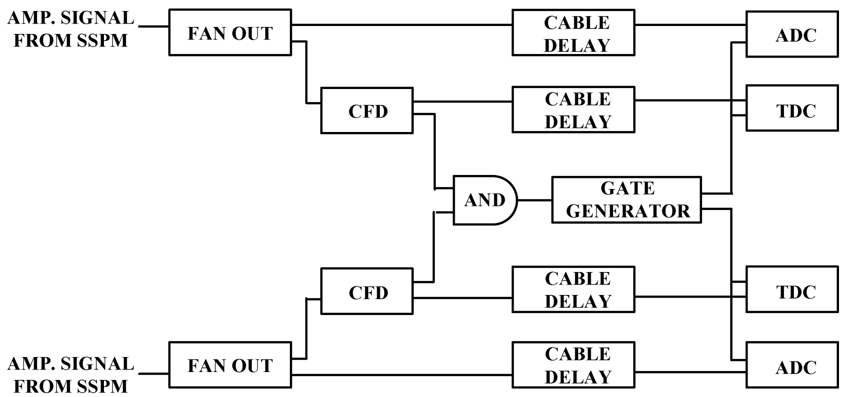

Fig. 1. Schematic diagram of data flow. “Amp. Signal” in the figure stands for “amplified signal.”

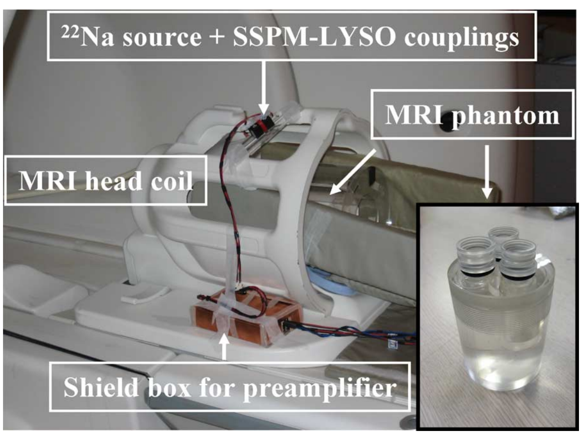

Fig. 2. SSPM-LYSO couplings and the copper-shielding box around the head coil.

arrangement also provided ample space for crystals and readout elements. Moreover, if the head coil is used for transmitting RF pulses and receiving MRI signals, this arrangement could simplify RF shielding since RF shielding has to ensure only the blocking of RF from the head coil.

The SSPM-LYSO couplings and the amplifier circuits were placed outside and inside the 3 T MRI, the positions of the SSPM-LYSO couplings and of the amplifier circuits enclosed in the copper-shield box outside the head coil, as shown in Fig. 2. When we tested the SSPM-LYSO couplings and the electronics board inside the 3 T MRI, they were always positioned at the center of the 3 T MRI. The energy and the coincidence time distributions were obtained with requiring coincidence of signals from the SSPM-LYSO couplings. We limited the number of coincidences to 5,000 events, such that the statistics of the events were the same as in the simultaneous acquisition of the SSPM-LYSO couplings and the MRI.

To check possible saturation with 511 keV photons, we built a SSPM-LYSO coupling and tested the dependence of charge on gamma-ray energy obtained with a variety of radiation sources ($^{99\mathrm{m}}$Tc : 140 keV, ^{131}I : 362 keV, ^{22}Na : 511 keV, and ^{137}Cs : 662 keV). The applied voltage to the SSPM-LYSO coupling was 29.8 V, the voltage recommended by the vendor for this particular device. The ADC charge was measured using the

TABLE II
PARAMETERS OF THE MRI PULSE SEQUENCES

Pulse sequence	Repetition time (ms)	Echo time (ms)	Flip angle
Spin echo, T1	500	9	90
Fast spin echo, T2	3500	120	90
Gradient echo, T2*	450	20	15

CAEN V965 ADC module with a 300 ns GATE generated from the SSPM-LYSO signal with a threshold of 30 mV. Except for this saturation test done at 25 °C, all the tests were performed inside the MRI room which maintains a stable temperature of 20 °C.

D. Simultaneous Acquisition of Data From SSPM-LYSO Couplings and 3 T MRI

Energy and coincidence time distributions, requiring coincidence of signals from the SSPM-LYSO couplings during T1, T2 and gradient echo T2* MRI pulse sequences were simultaneously obtained. Even though each MRI sequence lasted 2 minutes, the duration of SSPM data taking in each sequence was shorter than 2 minutes since we had to rely on manual coordination of data taking. RF pulses were generated by the body coil, and the head coil received MRI signals. A cylindrical phantom filled with water was positioned inside the head coil to evaluate MR images. Table II shows the parameters of the MRI pulse sequences used during simultaneous acquisition. The image matrix size and field of view for all the pulse sequences were 256 × 256 and 160 mm, respectively. The echo train length of the fast spin echo (T2) was 16.

III. RESULTS

A. Test Results of SSPM-LYSO Couplings Located Outside and Inside 3 T MRI

Fig. 3 represents the dependence to the charge on gamma-ray energy obtained with a variety of radiation sources ($^{99\mathrm{m}}$Tc : 140 keV, ^{131}I : 362 keV, ^{22}Na : 511 keV, and ^{137}Cs : 662 keV) and shows a good linear property within this gamma-ray energy range. The straight line in Fig. 3 represents a linear fit of data. Judging from Fig. 3, we are confident that the SSPMs used in this paper do not saturate with 511 keV photons.

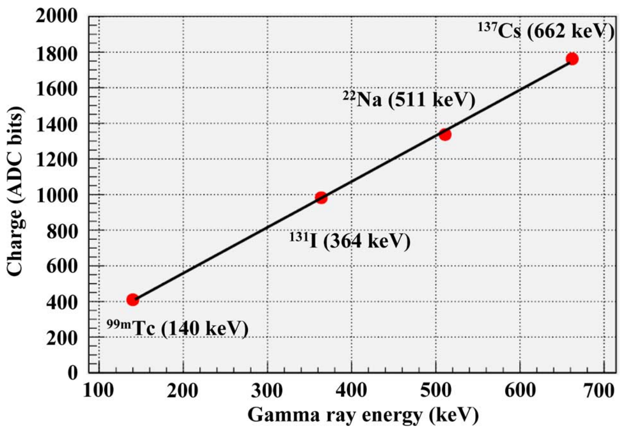

Fig. 3. Dependence of charge on gamma-ray energy obtained with a variety of radiation sources (^{99m}Tc : 140 keV, ^{131}I : 362 keV, ^{22}Na : 511 keV, and ^{137}Cs : 662 keV). The straight line represents a linear fit of data.

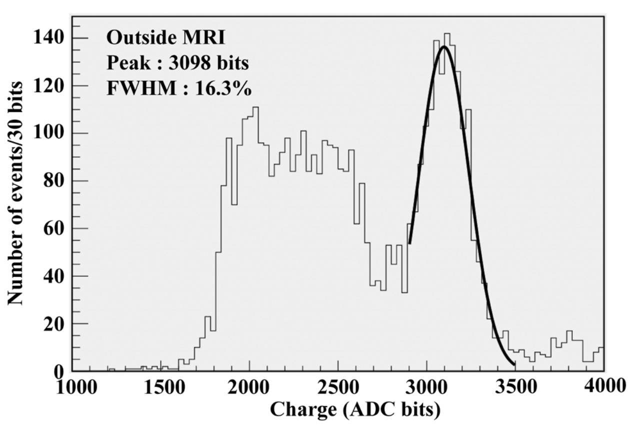

(a)

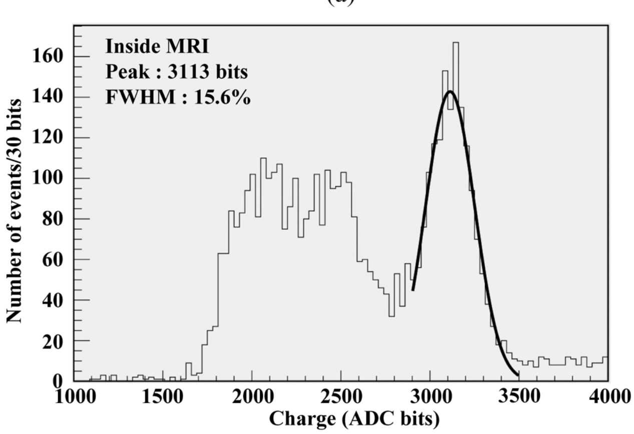

(b)

Fig. 4. Energy spectra of a SSPM-LYSO coupling obtained (a) outside and (b) inside the 3 T MRI scanner in the MRI room.

Fig. 4(a) and (b) respectively represent the energy distribution obtained from the SSPM-LYSO couplings outside and inside the 3 T MRI, and show almost no degradation of energy resolution. Energy resolution was 16.3% outside the 3 T MRI, and 15.6% inside. The energy resolutions were determined by fitting photoelectric peaks corresponding to 511 keV, assuming a Gaussian distribution. Since the fit errors of the energy resolutions were 0.7%, this difference is due to statistical limitations rather than improved energy resolution inside the 3 T MRI scanner. The fit ranges and the Gaussian curves are indicated by thick solid lines in histograms of Fig. 4(a) and (b). This energy resolution of 16.3% outside the MRI scanner is significantly better than that of SiPMs [12], and our measurements using a previous SSPM version [13]. The energy resolution obtained was slightly poorer than the 14.0% energy resolution obtained for APDs directly coupled to LSO crystals [7], but was much better than the 23.2% energy resolution of APDs coupled to LSO crystals using optical fibers [8]. The difference between Gaussian peak positions was negligible outside and inside the 3 T MRI. Fig. 4(a) and (b) show the energy distributions of one SSPM-LYSO coupling. The other SSPM-LYSO coupling gave similar distributions, even though energy resolutions outside (17.7%) and inside (15.7%) the MRI scanner were poorer.

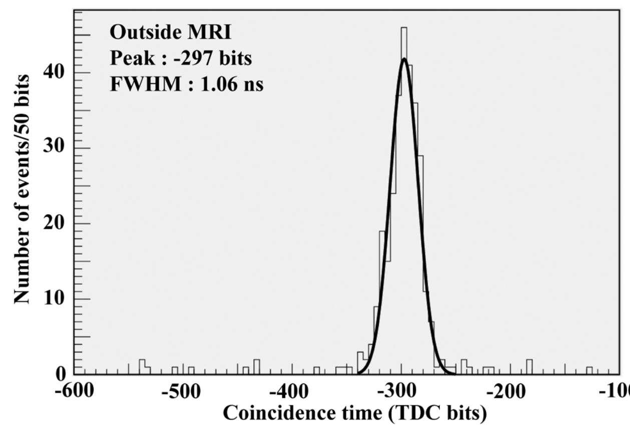

(a)

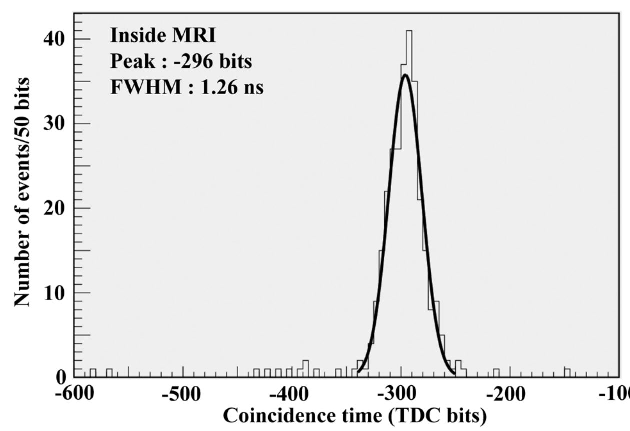

(b)

Fig. 5. Coincidence time distributions of two SSPMs obtained (a) outside and (b) inside the 3 T MRI scanner in the MRI room.

Fig. 5(a) and (b) show coincidence time distributions obtained from the SSPM-LYSO couplings outside and inside the 3 T MRI, respectively. Coincidence time resolutions were 1.06 ns outside and 1.26 ns inside the 3 T MRI. Time resolutions were obtained by fitting the coincidence time distribution assuming a Gaussian distribution. The fit ranges and the Gaussian curves are respectively indicated by thick solid lines in histograms. The fit errors of the coincidence time resolutions were 0.06 ns. The events in Fig. 5(a) and (b) were required to be in the Gaussian fit ranges shown in Fig. 4(a) and (b). The

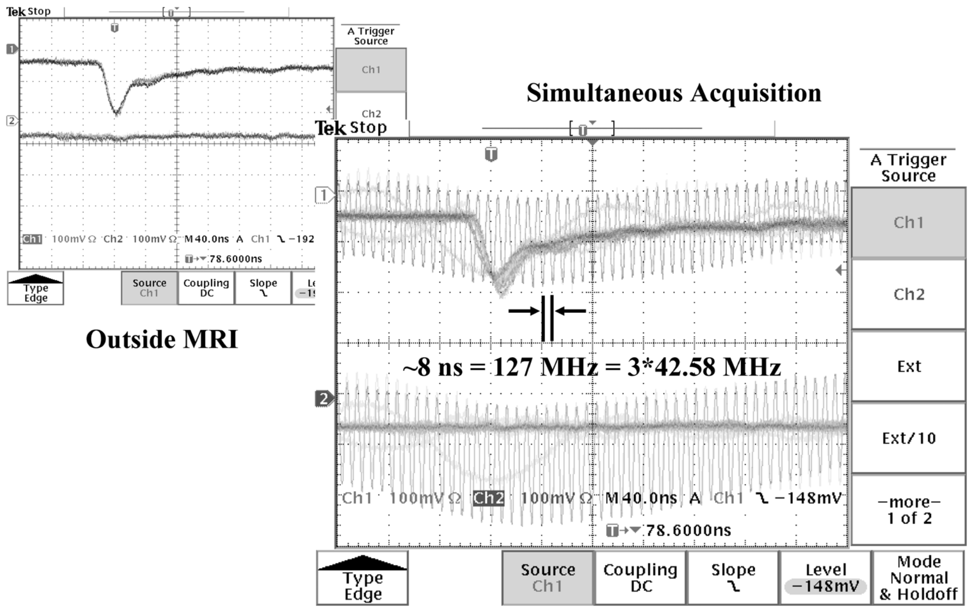

Fig. 6. Pulses from SSPM-LYSO couplings taken outside the 3 T MRI scanner and during the simultaneous acquisition of the spin echo T2 sequence.

excellent time resolution of 1.06 ns due to the fast rise time of the SSPMs was remarkable compared to the several ns of APDs [8]–[11]. Coincidence times and resolutions were only marginally different outside and inside the 3 T MRI scanner.

B. Test Results for Simultaneous Acquisitions From SSPM-LYSO Couplings and 3 T MRI

Fig. 6 shows the pulse shapes from SSPM-LYSO couplings taken with an oscilloscope (Tektronix, USA) outside the 3 T MRI, and during the T2 spin echo sequence inside the 3 T MRI scanner. The upper trace in each oscilloscope image shows the signal from the SSPM-LYSO coupling, while the lower trace represents the signal from the SSPM-LYSO coupling when the voltage to the SSPM-LYSO coupling was set at zero. The upper and lower oscilloscope traces taken during this simultaneous acquisition show characteristic RF pulses of 127 MHz from the 3 T MRI scanner. The characteristics of the RF pulses demonstrate the possibility of filtering out these RF pulses using notch or band filters if desired. It is also possible to not take data from SSPM-LYSO couplings during RF transmission. However, we did not examine this possibility during the present study.

Fig. 7(a) and (b) respectively show energy and coincidence time distributions of the SSPM-LYSO coupling obtained during simultaneous acquisition using the above-described gradient echo T2* sequence. A 15.0% energy resolution and a 1.18 ns coincidence time resolution were obtained for simultaneous acquisition. The 511-keV peak value of the photoelectric effect and the coincidence time were similar to those obtained outside the MRI scanner. The events in Fig. 7(b) were required to be in the Gaussian fit ranges shown in Fig. 7(a). We obtained similar energy and coincidence time resolutions of the SSPM-LYSO couplings during simultaneous acquisition using spin echo T1 and fast spin echo T2 sequences (Table III).

This energy resolution of 15.0% acquired while applying MRI pulse sequences is better than the 18% of APDs directly coupled to LSO crystals [7], and much better than the 24.1%

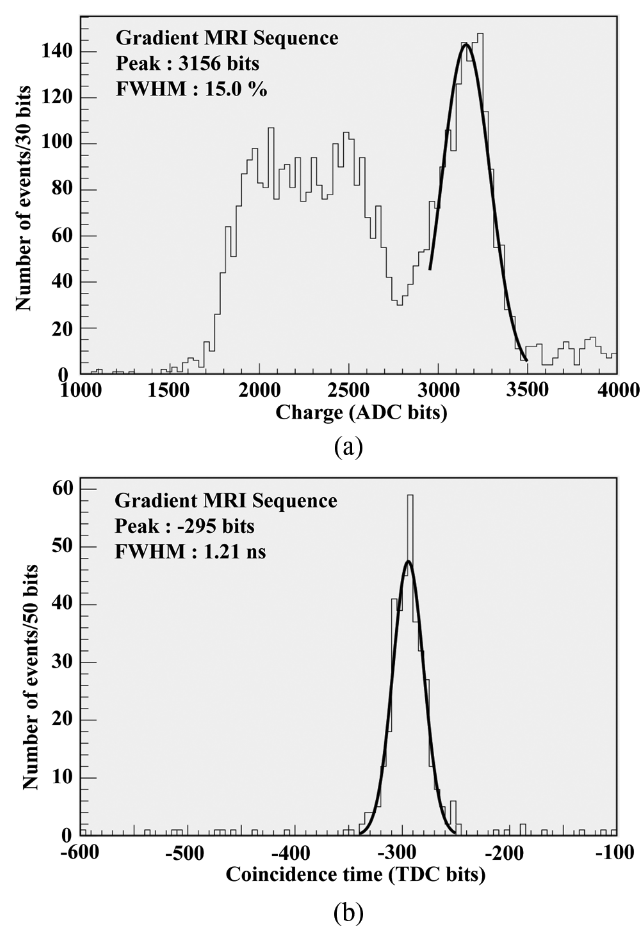

Fig. 7. ADC distribution of SSPM and coincidence time distributions of the two SSPMs obtained during the simultaneous acquisition of the gradient echo T2* sequence. (a) Outside and (b) inside the 3 T MRI scanner.

of APDs coupled to LSO crystals using optical fibers [8]. Although it is difficult to compare the coincidence time resolution

TABLE III
SUMMARY OF RESULTS SHOWING ENERGY AND COINCIDENCE TIME RESOLUTIONS OF BOTH SSPMS, ALONG WITH THE 511 keV PEAK VALUES AND COINCIDENCE TIMES. ADC VALUES ARE OFFSET-SUBTRACTED. ADC OFFSET VALUES WERE 1046 FOR CHANNEL 0 AND 1076 FOR CHANNEL 1, RESPECTIVELY. THE FIT ERRORS WERE ABOUT 1.0% FOR ENERGY RESOLUTIONS, AND ~0.1 ns FOR COINCIDENCE TIME RESOLUTIONS

Location/ MR sequence	511 keV peak value – Ch.0 (bit/ ratio)	511 keV resolution – Ch.0 (%, ratio)	511 keV peak value – Ch.1 (bit/ ratio)	511 keV resolution – Ch.1(%, ratio)	Coincidence time difference (bit/ratio)	Coincidence time resolution (ns/ratio)
Outside MRI (~0 T)/None	2052/1.00	16.3/1.00	1643/1.00	17.7/1.00	297/1.00	1.06/1.00
Inside MRI (3 T)/None	2067/1.01	15.6/0.96	1656/1.01	15.7/0.89	296/1.00	1.31/1.24
Inside MRI/Spin echo, T1	2180/1.06	16.5/1.01	1663/1.01	17.9/1.01	295/0.99	1.27/1.20
Inside MRI/Fast spin echo, T2	2113/1.03	15.9/0.98	1665/1.01	16.2/0.92	297/1.00	1.28/1.21
Inside MRI/Gradient echo, T2*	2110/1.03	15.0/0.92	1501/0.91	16.2/0.92	295/0.99	1.18/1.11

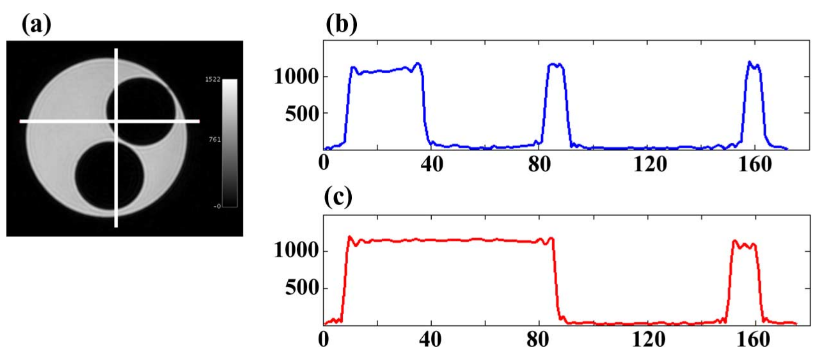

Fig. 8. MRI phantom image and its profiles shown by horizontal and vertical lines, obtained without SSPM-LYSO couplings or the copper-shielding box. (a) Phantom image; (b) horizontal and (c) vertical profiles.

of 1.18 ns obtained during the simultaneous acquisition of the gradient echo T2* sequence with the results from APDs coupled to scintillation crystals due to a lack of reported results, we do not doubt that this result is substantially better than that obtainable using APDs.

We have found that the performance of SSPM-LYSO couplings was not changed substantially, i.e., energy resolution of ~16% and coincidence time resolution of ~1.3 ns were maintained, by magnetic field strength and MRI pulse sequence differences. For SSPM-LYSO couplings to be useful for combined PET-MRI scanners, MR images should not be degraded appreciably during simultaneous acquisition. Fig. 8 shows an MR image of the water-filled phantom shown in Fig. 2, and its image profiles along the horizontal and vertical lines. The MR image in Fig. 8 was obtained without the SSPM-LYSO couplings or the shielding box. The MR image of the water-filled phantom, obtained during simultaneous acquisition using the gradient echo T2* sequence, is shown in Fig. 9, which also shows its image profiles along the horizontal and vertical lines. Figs. 8 and 9 show negligible differences in image profiles. We also obtained similar MR images for spin echo T1 and fast spin echo T2 sequences.

IV. SUMMARY AND CONCLUSION

In the present study, we measured the energy and coincidence time resolutions of SSPM-LYSO couplings outside a 3 T MRI scanner, and compared these with the results obtained inside the 3 T MRI scanner during T1, T2 and gradient echo T2* pulse sequences. Table III provides a summary of energy and coincidence time resolutions, along with 511 keV peak values of the photoelectric effect and coincidence times. These findings show that energy and coincidence time resolutions of LYSO-SSPM couplings do not strongly depend on magnetic field strength and the MR pulse sequence used. The energy resolutions during the MR pulse sequence were not degraded much because the MRI RF pulses did not coincide much with the coincidence events in the LYSO-SSPM couplings.

In the presence of the earth's magnetic field only, we obtained an energy resolution of 16.3%, which was better than the 21% previously reported for SiPMs [12] or the 25% reported for SSPMs [13]. This energy resolution is slightly poorer than the 14.0% reported for APDs directly coupled to LSO crystals [7], but much better than the 23.2% of APDs coupled to LSO

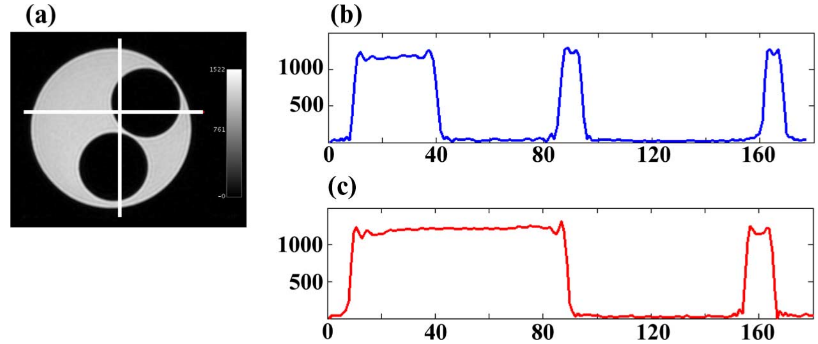

Fig. 9. MRI phantom image and its profiles shown by horizontal and vertical lines, obtained during the simultaneous acquisition of the gradient echo T2* sequence. The SSPM-LYSO couplings and the copper shielding box were present inside the 3 T MRI bore. (a) Phantom image; (b) horizontal and (c) vertical profiles.

crystals using optical fibers [8]. We also obtained a better coincidence time resolution of 1.06 ns than has been reported previously, i.e., 2.1 ns for SiPMs [12], 4.8 ns for SSPMs [13], and a handful of ns for APDs [8]–[11]. Recently, SiPMs with a sub-ns time resolution and 10$\sim$20% energy resolution were also reported [14], [15].

During the simultaneous acquisition of the gradient echo T2* sequence, an energy resolution of 15.0% is better than the 18% of APDs directly coupled to LSO crystals [7], and much better than the 24.1% of APDs coupled to LSO crystals by optical fibers [8]. Although it is difficult to compare the coincidence time resolution of 1.18 ns with the results from APDs coupled to scintillation crystals, due to a lack of reported results, we do not doubt that this result is substantially better than that achievable using APDs. We believe that SSPM-LYSO coupling results in better energy and coincidence time resolutions than APDs coupled to comparable crystals, due to their higher gain and rapid response times, especially in noisy environments, such as those within MRI scanners.

Considering that the small number of SSPM-LYSO couplings and electronics components placed in the MRI scanners during the present study, the observed negligible degradation of the MRI images may not be too surprising. However, the robust pulses of SSPM-LYSO couplings as compared with those of APDs may require thinner shielding to protect SSPM-LYSO couplings and readout electronics from RF and gradient pulses. Thinner shielding may improve MR images since gradient and RF pulses, due to thinner shielding, should then reach objects being imaged without significant loss.

Even though the number of triggered events in each case was 5000 events taken over less than 2 minutes resulting in the $\sim$5% fitting errors of energy and coincidence time resolutions, we did not try to take more events with this experimental setup. Energy and timing resolutions of the PET system in a combined PET and MRI would depend on a lot of factors, such as the RF shielding, and RF and noise pickups to electronics and cables. This simple experimental setup is too limited to study these complicated issues.

In conclusion, the present study demonstrates that SSPMs have excellent potential for use in combined PET-MRI scanners.

References

[1] J. Barentsz, S. Takahashi, W. Oyen, R. Mus, P. D. Mulder, R. Reznek, M. Oudkerk, and W. Mali, "Commonly used imaging techniques for diagnosis and staging," *J. Clin. Oncol.*, vol. 24, pp. 3234–3244, 2006.

[2] J. Gaa, E. J. Rummeny, and M. D. Seemann, "Whole-body imaging with PET/MRI," *Eur. J. Med. Res.*, vol. 9, pp. 309–312, 2004.

[3] M. D. Seemann, "Whole-body PET/MRI: The future in oncological imaging," *Technol. Cancer Res. Treat.*, vol. 4, pp. 577–582, 2005.

[4] Y. Shao, S. R. Cherry, K. Farahani, K. Meadors, S. Siegel, R. W. Silverman, and P. K. Marsden, "Simultaneous PET and MR imaging," *Phys. Med. Biol.*, vol. 42, pp. 1965–1970, 1997.

[5] P. K. Marsden, D. Strul, S. F. Keevil, S. C. Williams, and D. Cash, "Simultaneous PET and NMR," *Br. J. Radiol.*, vol. 75, pp. S53–S59, 2002.

[6] B. Pichler, E. Lorenz, R. Mirzoyan, W. Pimp, F. Roder, M. Schwaiger, and S. I. Ziegler, "Performance test of a LSO-APD PET module in a 9.4 Tesla magnet," in *Proc. IEEE NSS-MIC Conf.*, 1997, pp. 1237–1239.

[7] B. J. Pichler, M. S. Judenhofer, C. Catana, J. H. Walton, M. Kneilling, R. E. Nutt, S. B. Siegel, C. D. Claussen, and S. R. Cherry, "Performance test of an LSO-APD detector in a 7-T MRI scanner for simultaneous PET/MRI," *J. Nucl. Med.*, vol. 47, pp. 639–647, 2006.

[8] C. Catana, Y. Wu, M. S. Judenhofer, J. Qi, B. J. Pichler, and S. R. Cherry, "Simultaneous acquisition of multislice PET and MR images: Initial results with a MR-compatible PET scanner," *J. Nucl. Med.*, vol. 47, pp. 1968–1976, 2006.

[9] D. Schlyer, P. Vaska, C. Woody, D. Tomasi, S. Southekal, S. Solis-Najera, S. Stoll, J. Pratte, S. Junnarkar, S. Krishnamoothy, M. Purschke, S. Park, S. Maramraju, and A. Kriplani, "First image from the BNL simultaneous PET/MRI scanner," *J. Nucl. Med.*, vol. 48, no. suppl. 1, p. 289, 2007.

[10] M. Schmand, Z. Burbar, J. L. Corbeil, N. Zhang, C. Michael, L. Byars, L. Eriksson, R. Grazioso, M. Martin, A. Moor, J. Camp, V. Matschl, R. Ladebeck, W. Renz, H. Fischer, K. Jattke, G. Schnur, N. Rietsch, B. Bendriem, and W. Heiss, "BrainPET: First human tomograph for simultaneous (functional) PET and MR imaging," *J. Nucl. Med.*, vol. 48, no. suppl. 1, p. 245, 2007.

[11] H. Schlemmer, B. J. Pichler, K. Wienhard, M. Schmand, C. Nahmias, D. Townsend, W. Heiss, and C. D. Claussen, "Simultaneous MR/PET for brain imaging: First patient scans," *J. Nucl. Med.*, vol. 48, no. suppl. 1, p. 245, 2007.

[12] A. N. Otte, J. Barral, B. Dolgoshein, J. Hose, S. Klemin, E. Lorenz, R. Mirzoyan, E. Popov, and M. Teshima, "A test of silicon photomultipliers as readout for PET," *Nucl. Instrum. Meth. A.*, vol. 545, pp. 705–715, 2005.

[13] J. S. Lee, M. Ito, K. S. Sim, B. Hong, K. S. Lee, J. Muhammad, J. T. Rhee, G. S. Lee, K. S. Park, I. C. Song, and S. J. Hong, "Investigation of solid state photomultipliers for positron emission tomography scanners," *J. Korean Phys. Soc.*, vol. 50, pp. 1332–1339, 2007.

[14] M. Szawlowski, D. Meier, G. Maehlum, D. J. Wagenaar, and B. E. Patt, "Spectroscopy and timing with Multi-Pixel Photon Counters (MPPC) and LYSO scintillators," in *Nucl. Sci. Symp. Conf. Record*, 2007, vol. 6, pp. 4591–4596.

[15] K. C. Burr and W. Gin-Chung, "Scintillation detection using 3 mm $\times$ 3 mm silicon photomultipliers," in *Nucl. Sci. Symp. Conf. Record*, 2007, vol. 2, pp. 975–982.